

Anomalous Differences of Light Elements in Determining Precise Binding Modes of Ligands to Glycerol-3-Phosphate Dehydrogenase

Jungwoo Choe,^{1,2} Stephen Suresh,^{3,6}
Goragot Wisedchaisri,¹ Kevin J. Kennedy,^{4,7}
Michael H. Gelb,⁴ and Wim G.J. Hol^{1,3,5}

¹Department of Biochemistry

²Biomolecular Structure and Design (BMSD)
Graduate Student Program

³Howard Hughes Medical Institute

⁴Department of Chemistry and Biochemistry
University of Washington
Seattle, Washington 98195

Summary

Pathogenic protozoa such as *Trypanosoma* and *Leishmania* species cause tremendous suffering worldwide. Because of their dependence on glycolysis for energy, the glycolytic enzymes of these organisms, including glycerol-3-phosphate dehydrogenase (GPDH), are considered attractive drug targets. Using the adenine part of NAD as a lead compound, several 2,6-disubstituted purines were synthesized as inhibitors of *Leishmania mexicana* GPDH (*Lm*GPDH). The electron densities for the inhibitor 2-bromo-6-chloro-purine bound to *Lm*GPDH using a “conventional” wavelength around 1 Å displayed a quasisymmetric shape. The anomalous signals from data collected at 1.77 Å clearly indicated the positions of the halogen atoms and revealed the multiple binding modes of this inhibitor. Intriguing differences in the observed binding modes of the inhibitor between very similarly prepared crystals illustrate the possibility of crystal-to-crystal variations in protein-ligand complex structures.

Introduction

Pathogenic protozoa, such as *Trypanosoma brucei*, the causative agent of sleeping sickness, and several *Leishmania* species, responsible for various forms of leishmaniasis, continue to cause tremendous suffering and mortality to both people and livestock [1]. Moreover, the drugs currently in use to treat the diseases are often severely hampered by problems like toxicity and resistance [2]. There is therefore an urgent need for more effective drugs. Our laboratory has been studying the glycolytic enzymes of these parasites as drug targets with the aim of inhibiting glycolysis and thereby killing the parasites [3–14]. The glycolytic enzymes are attractive drug targets for diseases caused by trypanosomatids since glycolysis is the major source of energy for most of these parasites during the mammalian stage of their life cycle. For example, the bloodstream form of *T. brucei* is entirely dependent on glycolysis for ATP production, as it lacks a functional tricarboxylic acid

cycle [15, 16]. Computer modeling studies support the feasibility of blocking glycolysis by inhibiting the glycolytic enzymes [17–20]. The sequences and structures of the glycolytic enzymes from trypanosome and leishmania species are often very similar to each other and different from the human homolog, enabling the design of selective inhibitors that inhibit parasite enzymes but affect the human enzymes to a considerably lesser degree [10, 11, 14, 21].

The enzyme NAD-dependent glycerol-3-phosphate dehydrogenase (GPDH, E.C. 1.1.1.8) catalyzes the interconversion of dihydroxy acetone phosphate (DHAP) and glycerol-3-phosphate (G3P) using NAD as a cosubstrate. In the bloodstream form of *T. brucei*, GPDH is especially important because it is responsible for maintaining the NAD/NADH balance in the glycosome by the oxidation of the NADH produced by glyceraldehyde-3-phosphate dehydrogenase during glycolysis. Blocking GPDH would jeopardize ATP production and also lead to the accumulation of DHAP in the glycosome, which may spontaneously convert to methylglyoxylate, a toxic compound that reacts nonspecifically with proteins [22, 23]. The importance of this enzyme in *Leishmania* species is yet to be evaluated, owing to the presence of an active mitochondrion throughout the *Leishmania* life cycle [24]. GPDH in *Leishmania*, however, plays an important role in utilizing the glycerol liberated from neutral lipids, especially in amastigote stages, where fatty acids rather than carbohydrates are predominantly used as an energy source [25]. *L. mexicana* GPDH (*Lm*GPDH) shares 63% sequence identity with the *T. brucei* enzyme and could serve as a model for drug design targeting *T. brucei* GPDH [25]. The apo and NADH bound structures of *Lm*GPDH were previously determined in our laboratory [13]. When the amino acid sequences near the substrate binding sites of *L. mexicana* and human GPDH were compared for the possibility of selective inhibitor design, the region close to the adenine part of NAD(H) showed substantial differences between the parasite and host enzymes, whereas the DHAP/G3P binding site is more highly conserved [13]. In the next step toward developing selective inhibitors, 2,6-disubstituted purine analogs were synthesized, and some of them showed inhibition of *T. brucei* GPDH with an IC₅₀ of 5 mM. Here we report the crystal structures of *Lm*GPDH in complex with 2-fluoro-6-chloro-purine (FCP), 2-bromo-6-chloro-purine (BCP), and 2-bromo-6-hydroxy-purine (BOP). These molecules may serve as lead compounds to explore the adenosine binding pocket of *Lm*GPDH.

Determining the exact binding mode of ligands to macromolecular targets can be particularly challenging when the ligands are quasisymmetric or adopt multiple binding modes. By carefully selecting wavelengths, anomalous differences of light elements in protein crystallographic data sets can be used to locate and orient ligands, such as substrate, inhibitor, and metal ions bound to proteins [26–28]. The position of weak anomalous scatterers can be determined from the Bijvoet

⁵ Correspondence: hol@gouda.bmsc.washington.edu

⁶ Present address: Structural Genomix, San Diego, California 92121.

⁷ Present address: MediQuest Therapeutics Inc., Seattle, Washington 98103.

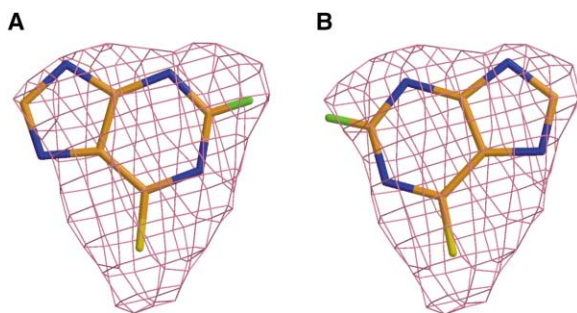


Figure 1. Model-Unbiased, SigmaA-Weighted Fo-Fc Map of FCP Bound to *L. mexicana* Glycerol-3-Phosphate Dehydrogenase at 2.2 Å Contoured at 2.5 σ

(A) Orientation 1 and (B) Orientation 2. Carbon, nitrogen, chlorine, and fluorine are colored brown, blue, yellow, and green, respectively. Drawn using MOLSCRIPT [45].

anomalous difference Fourier map, once reasonably accurate phases have been obtained. The ambiguities in the binding modes of inhibitor bound to *LmGPDH* could be resolved with the help of the anomalous signal obtained from Br or Cl atoms that were incorporated in the inhibitors.

Results and Discussion

2,6-Disubstituted Purine as an Inhibitor of *LmGPDH*

Based on the binding mode of NADH in the crystal structure of the *LmGPDH*:NADH complex [13], the purine ring of NADH was first explored for substitution at the 2 and 6 positions. A small number of 2,6-dihalogenated purines with IC_{50} 's of about 5 mM were synthesized and

showed significantly higher inhibition of *LmGPDH* than adenine. Before further developing high-affinity inhibitors, the binding modes of three 2,6-dihalogenated purine compounds (FCP, BCP, and BOP) were determined by X-ray crystallography to understand the exact binding modes of these lead compounds. The crystal structures showed that these three inhibitors are binding generally in the same region as the adenosine part of NADH, but the binding mode of each compound differs significantly from that of adenosine part of NADH.

Binding Modes of FCP

Even though the electron density for the inhibitor FCP in the difference map is clear and significant, closer inspection revealed that there are two possible orientations of the bound FCP that are compatible with the electron density (Figure 1). The position of Cl of the bound FCP can be determined unequivocally since Cl with its 17 electrons gave rise to the highest peak in the difference density with a height of 8.2 σ . With the position of the Cl fixed, there were two possible ways by which FCP could fit into the rather symmetrical triangular density (Figure 1). Both orientations were independently refined and analyzed. Although one of the orientations had slightly lower temperature factors than the other, the available data makes it difficult to establish with certainty the true orientation of this ligand, and it is also possible that both orientations are present in the crystal.

Binding Modes of BCP

BCP was synthesized to solve the ambiguity in the binding mode of FCP by incorporating two heavy atoms (Br and Cl) to differentiate them from carbons and nitrogens. The structure was first solved using data from the Advance Light Source (ALS, Berkeley) collected at 0.979 Å

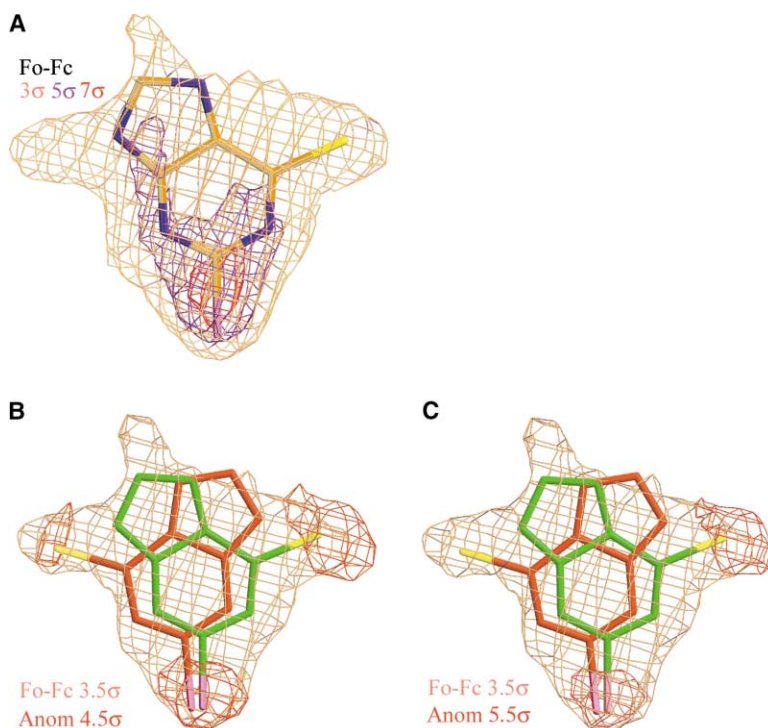


Figure 2. Electron Densities of the Bound Inhibitor BCP

(A) Model-unbiased, sigmaA-weighted Fo-Fc map contoured at 3 σ (light brown), 5 σ (violet), and 7 σ (red) with conformation A of BCP.

(B and C) Two alternative conformations (conformation A, green; conformation B, red) of BCP bound to *L. mexicana* GPDH in a model-unbiased, sigmaA-weighted Fo-Fc map (B) contoured at 3.5 σ (light brown) and an anomalous difference Fourier map contoured at 4.5 σ (red) and (C) an anomalous difference Fourier map contoured at 5.5 σ (red). Carbon, nitrogen, chlorine, and bromine are colored brown, blue, yellow, and pink, respectively. Drawn using MOLSCRIPT [45] and Raster3D [46].

wavelength. The Fo-Fc density clearly showed the presence of bound inhibitor, and at 7σ , only one peak appeared at the “lower” corner of a triangular density. This peak was taken as the position of the Br atom, because with its 35 electrons, Br was the heaviest element in the inhibitor (Figure 2A). But the position of Cl, even with its 17 electrons, was not obvious from the Fo-Fc density maps displayed at various contour levels.

To locate the Cl and establish the precise binding mode of the inhibitor, data were collected at the Advanced Photon Source (APS, Argonne National Laboratory) using 1.7712 Å wavelength X-rays with an overall redundancy of 12.9 to measure the anomalous signals from Br and Cl. The anomalous difference density, calculated after a few rounds of positional refinement when the R factor had dropped to 21.2%, showed distinct peaks inside the Fo-Fc density of the inhibitor. When contoured at the 4.4σ level, anomalous density was visible at three positions, one at each corner of the triangular shaped Fo-Fc density. This suggested that BCP has two alternative binding modes that are rotated 180° about the Br-C2 bond with the Br at the same position. The peak height of the anomalous density at the “upper left” corner was 5.2σ and that of the “upper right” corner was 7.1σ . This indicated that binding mode A (Figures 2B and 2C, green) has a higher occupancy than binding mode B (Figures 2B and 2C, red). The occupancy refinement by CNS [29] showed that binding mode A has an occupancy of 0.7 and binding mode B an occupancy of 0.3, with comparable average B factors for the alternative conformations.

Sulfur Peaks and the Second Binding Site of BCP from 1.77 Å BCP Data Sets

When the Bijvoet anomalous difference Fourier map was calculated for the *Lm*GPDH:BCP complex, it also showed peaks from the sulfur atoms of the protein in addition to the halogen atoms of the BCP. The expected average ratio $\langle |\Delta F_A| \rangle / \langle F \rangle$ can be calculated from the equation $2^{1/2}(N_A^{1/2}\Delta f_A^{\text{eff}}) / (N_P^{1/2}Z_{\text{eff}})$ [30]. In the case of the *Lm*GPDH:BCP complex, the 18 anomalous scatterers, including one Br with $\Delta f_A^{\text{eff}} = 1.640$, one Cl with $\Delta f_A^{\text{eff}} = 0.905$ electrons from BCP, and 16 S's with $\Delta f_A^{\text{eff}} = 0.722$ electrons from the cysteine and methionine residues of the protein [31, 32], give a value of 2.24% for the ratio of $\langle |\Delta F_A| \rangle / \langle F \rangle$ at 1.7712 Å wavelength. The experimentally observed $\langle |\Delta F_A| \rangle / \langle F \rangle$ ratio of BCP data is lower or close to the expected value in the resolution range from 50 to 2.7 Å (Figure 3B). The observed ratio increased at higher resolution, probably owing to the increase in errors of the ΔF_A and F measurements.

The anomalous difference Fourier map for the whole protein region was calculated to 2.7 Å resolution using the data collected at 1.77 Å wavelength (Figure 3A). The peak search program PEAKMAX [33] was used to locate the peaks in the anomalous difference Fourier map. Inspection of the maps revealed that the anomalous difference Fourier map calculated between 50–2.7 Å showed the highest number of peaks that coincide with the anomalous scatterers while displaying the lowest number of noise peaks. The map calculated between 50 and 2.7 Å showed peaks for the Br and Cl atoms of the

inhibitor as well as for 11 out of 16 sulfurs in the protein, with 5 noise peaks above 4σ (Table 1). The peak heights of S atoms in the anomalous difference Fourier map are inversely correlated to the refined B factors (Table 1).

Surprisingly, the highest peak in the anomalous difference Fourier map was not from one of the anomalous scatterers mentioned above. The strongest peak appeared on the surface of the protein close to the side chains of Leu339 and the methylene groups of Arg336 and carbonyl oxygen of Arg336. The distances from the center of the peak to the carbons range from 3.9 to 4.3 Å and that to the carbonyl oxygen of Arg336 is 3.4 Å (Figure 3C). When a water molecule is placed in the “mystery” density, its B factor was refined to 14 \AA^2 , suggesting it is not a very heavy element with a strong anomalous signal at 1.77 Å wavelength. There is a spherical Fo-Fc density overlapping the mystery peak in the anomalous difference density. There is a room for an inhibitor molecule at this site, but the Fo-Fc map does not show clear evidence of this.

To determine the identity of the mystery peak at the secondary binding sites, a second data set was collected at 1.77 Å wavelength using another crystal prepared in the same way. The resulting Fo-Fc difference map showed two densities indicating the presence of two BCP molecules stacked on top of each other, BCP2 and BCP3 for the “lower” and “upper” difference densities, respectively (Figure 3D). There were also anomalous densities at one corner of the each difference density with heights of 4.8σ and 4.2σ for the lower and upper difference densities, respectively (Figure 3D). The distance between the anomalous density of BCP2 and the mystery peak from the first data set was about 0.4 Å. This binding site is created by symmetry-related molecules. The observed anomalous density in each difference density is thought to be from the Br atom of the inhibitor, but the anomalous density from the Cl atoms is not observed, probably because of the relatively low occupancy of the molecules.

From these observations from the second crystal, a possible explanation for the strong anomalous density of the first *Lm*GPDH:BCP crystal is that the BCP molecule has multiple binding modes spanning the large secondary binding site formed between two protein molecules, with the Br atom positioned where the anomalous density is observed. The precise shape of this binding site may determine how many BCP molecules fit into this cavity, and hence the number of BCP molecules and the shape of the densities might be very sensitive to small crystal-to-crystal differences and also to the molecular rearrangements during the cryocooling process.

Binding Mode of BOP

The data for BOP was collected at 0.91942 Å to maximize the anomalous signal from Br. A peak from the anomalous difference density appeared in the Fo-Fc density of BOP, indicating the position of Br in BOP. This anomalous difference peak was clearly visible even at the 10σ level and was the only peak in the whole protein region at this contour level (Figure 4). With only one anomalous scatterer (Br) in BOP, the anomalous difference Fourier

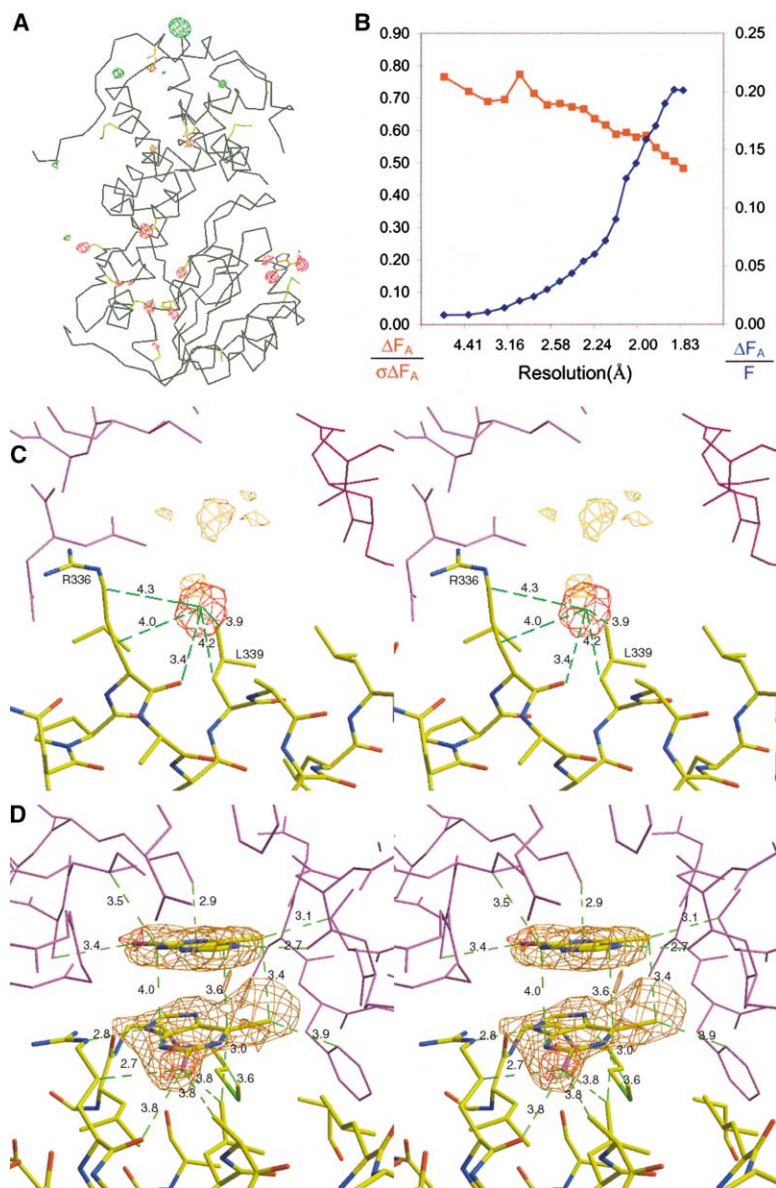


Figure 3. Anomalous Difference Densities from the Whole Protein and the Secondary Binding Site of BCP

(A) The anomalous difference Fourier map contoured at 4.0σ for the whole protein region calculated from 50 to 2.7 Å. The peaks that coincide with anomalous scatterers are colored red, and those that do not are colored green. The inhibitor and the side chains of all cysteine and methionine residues are shown together with the C^α model of *LmGPDH* (B) statistics of the anomalous signal in the data. (C) The anomalous difference Fourier map contoured at 10σ (red) and Fo-Fc map contoured at 3σ (light brown) calculated from 50 to 2.7 Å around the unidentified peak from data set BCP1. The distances from the center of the unidentified peak and neighboring residues are indicated. Symmetry mates are drawn in violet. (D) The anomalous difference Fourier map contoured at 3.5σ (red) and model-unbiased, sigmaA-weighted Fo-Fc map contoured at 3σ (light brown) calculated from 50 to 2.5 Å from data set BCP2. The two BCP molecules (BCP2: lower density, BCP3: upper density) are also shown.

map does not give information whether BOP is adopting alternative binding modes. The Fo-Fc difference density seems to indicate only one binding mode where the hydroxyl group at the 6 position is pointing in the same direction as the Cl of BCP in its preferred conformation (Figure 2, orientation A).

Comparison of Binding Modes of Inhibitors with NADH

The overall structures of the *LmGPDH* complexed with NADH, BCP, BOP, and FCP are very similar to each other, and 346 C^α atoms superpose with rmsd's ranging from 0.22 to 0.37 Å. Yet, the side chains of M46 and F97 residues that make the hydrophobic cleft show flexibility and shift as much as 1.0 Å upon binding different ligands (Figure 5B). When compared to NADH, the three inhibitors are bound deeper into the hydrophobic cleft, with the halogen atoms occupying a hydrophobic pocket created by W44, I93, and F101 (Figure 5A). Calculation

of the buried surface area by the program Naccess (Department of Biochemistry and Molecular Biology, University College, London) with a probe radius of 1.4 Å showed that the buried surface areas for BCP conformation A, BCP conformation B, BOP, FCP, and the adenine ring of NADH are 199, 203, 172, 179, and 125 Å², respectively (Figure 5D).

The BCP and BOP molecules bind to *LmGPDH* in quite similar ways where the purine rings of BCP and BOP are rotated and shifted with respect to the purine ring of adenosine such that the ring resides deep in the cleft with the Br atom at the 2 position reaching a hydrophobic pocket made by W44, I93, and F101. This pocket cannot be completely filled by the adenine ring of NADH due to the constraint from the rest of the NADH molecule. The FCP adopts yet another binding mode, with the Cl atom at the 6 position deep in the cleft pointing toward the protein instead of pointing to the solvent as in NADH. Despite the differences of the bind-

Table 1. Results of Peak Searching of a Bijvoet Anomalous Difference Fourier Map and Refined B Factors of the Anomalous Scatterers from Data Set BCP1

Atom Name	Peak Height (σ)	B Factor (\AA^2)
Unknown	20.3	17.2
S $_{\gamma}$ of Cys203	7.5	17.8
Cl of BCP in conformation A	7.1	52.2
Br of BCP	6.7	68.9
S δ of Met185	6.4	23.3
S $_{\gamma}$ of Cys167	6.0	19.7
Cl of BCP in conformation B	5.2	53.3
S δ of Met32	5.1	29.3
S δ of Met319	5.0	21.0
S $_{\gamma}$ of Cys123	4.9	22.7
Noise	4.6	–
S $_{\gamma}$ of Cys194	4.4	23.0
S $_{\gamma}$ of Cys322	4.3	22.3
S $_{\gamma}$ of Cys38	4.3	24.9
S δ of Met225	4.3	35.6
Noise	4.3	–
S $_{\gamma}$ of Cys268	4.2	23.4
Noise	4.1	–
Noise	4.0	–
Noise ^a	4.0	–
S δ of Met235 ^a	3.3	29.6
S $_{\gamma}$ of Cys42 ^a	3.2	34.4
S δ of Met309 ^a	2.8	42.8
S δ of Met46 ^a	1.1	51.0
S $_{\gamma}$ of Cys345 ^a	1.1	55.8

^aBelow 4 σ level, more noise peaks occur that are not listed.

ing modes, all three planar inhibitors are confined to the same plane between F97 and M46. The N1 atom of BCP and the N7 atom of FCP make hydrogen bonds with a water molecule that is also coordinated to the backbone carbonyl oxygen of F97 and backbone amide of F101. There are significant differences between human and *T. brucei* GPDH around the adenosine binding site, which can be exploited for selective inhibitor design (Figure 5C).

Significance

Determination of the binding mode of small organic molecules bound to a macromolecule by X-ray crystal-

lography can be challenging for various reasons, such as low resolution of the data, low occupancy of the bound ligand, multiple binding modes, and the quasi-symmetric shape of the molecule. Anomalous scatterers within the ligand can be used as a tool to locate and orient the molecule and to establish the binding mode. Many biologically active small molecules contain elements that can give small but significant anomalous signal, such as P, S, Cl, and Br. In the Comprehensive Medicinal Chemistry database (MDL Information Systems, San Leandro, CA), about 11% of the drugs contain S and about 16% contain Cl. As illustrated in this paper, anomalous signals from these elements can help determine the precise binding mode of small molecules. Furthermore, by using the different absorption edges of the elements, one can differentiate elements that bind in similar environments. Finally, the observed variations of conventional and anomalous difference maps derived from similarly prepared crystals are a reason to be cautious with the interpretation of crystallographic results from a single crystal structure.

Experimental Procedures

Synthesis of 2,6-Disubstituted Adenine Analogs

2-bromo-6-hydroxy-purine (BOP) was made by bromination of commercially available 2-thioxanthine (TCI America) according to a previously described method [34]. The product was then treated with POCl₃ to give 2-bromo-6-chloro-purine (BCP) [35]. 2-fluoro-6-chloro-purine was made from 2-amino-6-chloro-purine by diazotization with sodium nitrite in aqueous fluoroboric acid [36].

Overexpression and Purification of *Lm*GPDH

Leishmania mexicana glycerol-3-phosphate dehydrogenase (*Lm*GPDH) was overexpressed in *E. coli* as previously described [37]. The protein was subsequently purified in a single step using a SPRINT HS20 cation exchange column. The resulting protein was

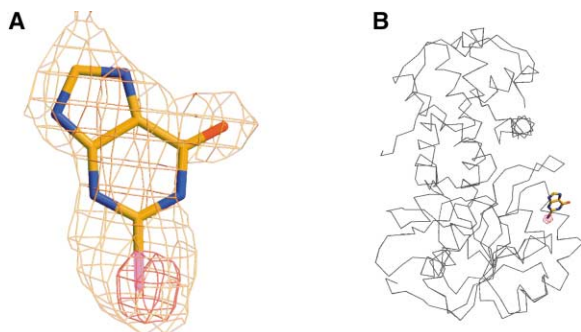
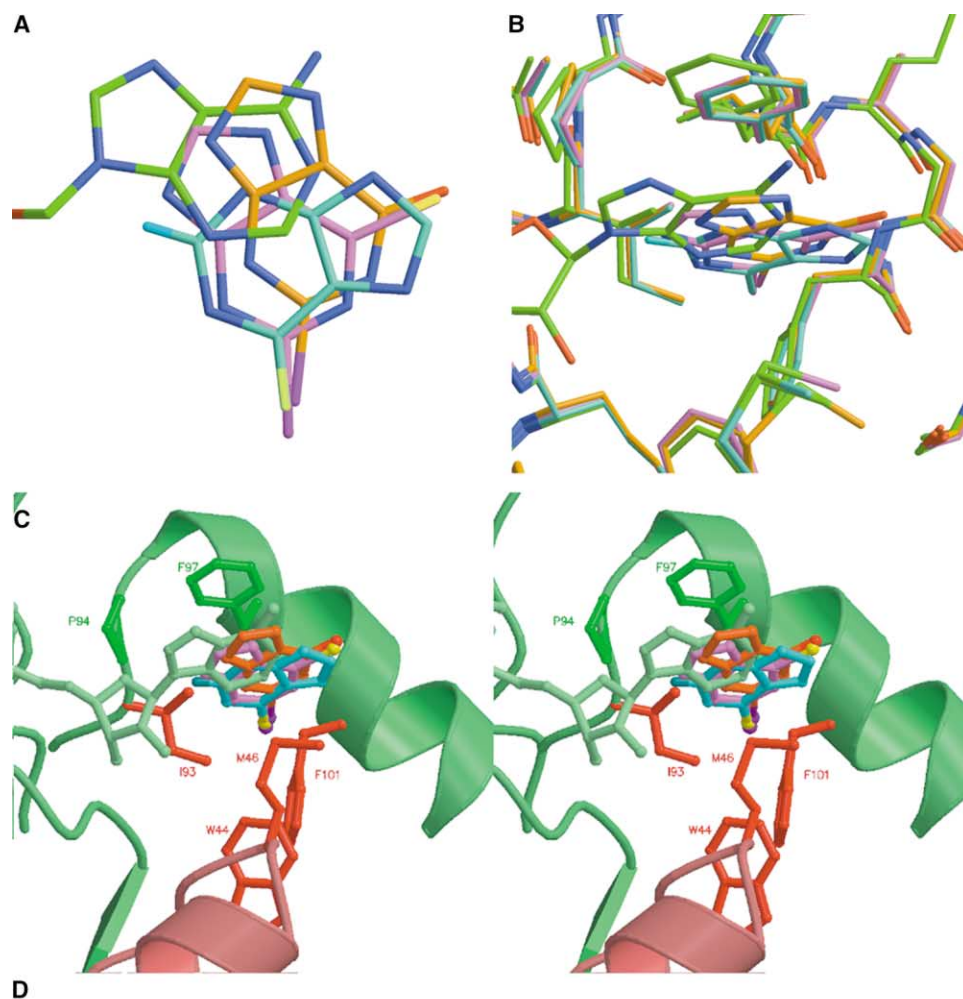


Figure 4. Electron Densities for the Bound Inhibitor BOP
(A) Model-unbiased, sigmaA-weighted Fo-Fc map of BOP bound to *Lm*GPDH contoured at 2.4 σ (pink) and the anomalous difference Fourier map (red) contoured at 10 σ superimposed with the final model of BOP.
(B) The anomalous difference Fourier map (red) contoured at 10 σ for the whole protein region drawn with the C $^{\alpha}$ model of the *Lm*GPDH and inhibitor BOP. Carbon, nitrogen, oxygen, and bromine are colored brown, blue, red, and pink, respectively.



		Total (\AA^2)	Non-polar (\AA^2)	Polar (\AA^2)
Adenine in NADH		125.0	86.4	38.6
FCP		179.1	116.5	62.6
BCP	Binding mode A	199.4	160.7	38.7
	Binding mode B	203.0	169.6	33.5
BOP		172.5	136.0	36.6

Figure 5. Comparison of Binding Modes of NADH and Bound Inhibitors

(A) Superposition of NADH, FCP, BCP, and BOP from corresponding complex structures with *LmGPDH*. The carbons of NADH are colored green, FCP cyan, BCP pink, and BOP orange. Nitrogens, oxygen, fluorine, chlorine and bromine are colored blue, red, dark cyan, yellow, and violet, respectively.

(B) Another view of (A) with the surrounding residue.

(C) Stereoview of the superposition where conserved residues between trypanosomatid (*L. mexicana* and *T. brucei*) and human GPDH are colored green, while residues that are different shown in red. An α helix containing residues 37–48 is also colored red, where an insertion and considerable sequence differences occur in the human enzymes compared to the trypanosomatid enzymes.

(D) Buried surface area calculated by the program Naccess.

concentrated to 4 mg/ml and dialysed against buffer containing 20 mM triethanolamine (TEA) (pH 7.2), 4 mM DTT, 1 mM EDTA, and 0.5 mM Pefabloc.

Inhibition Studies

Assays were performed in a total volume of 0.5 ml reaction mixture consisting of 0.1 M TEA buffer (pH 7.5), 0.60 mM NAD^+ , and 10.27

mM glycerol 3-phosphate at 23°C. Compounds were dissolved in DMSO and tested at maximum solubility, keeping DMSO concentration in the assay at 5%. Reactions were initiated by the addition of excess *T. brucei* GPDH, and activity was measured in the direction of NADH formation by monitoring absorption at 340 nm. Control reactions were run in 5% DMSO without added inhibitor, and inhibition was measured as percent of control using the initial velocities

Table 2. Data Collection and Refinement Statistics

	FCP	BOP	BCP1	BCP2
Space group	P4 ₁ 2 ₁ 2	P4 ₁ 2 ₁ 2	P4 ₁ 2 ₁ 2	P4 ₁ 2 ₁ 2
Cell parameters (Å)	A = b = 70.3, c = 210.9	a = b = 70.5, c = 211.7	a = b = 70.4, c = 210.8	a = b = 70.4, c = 210.9
Resolution (Å)	2.2	2.5	1.9	2.5
Data processing				
Observations	196124	295254	532171	286843
Unique reflections	27686	19175	41189	18150
Redundancy	7.1	15.4	12.9	15.8
I/σ(I)	27.0 (7.6)	34.4 (4.4)	36.8 (3.1)	5.0 (1.6)
Completeness (%)	99.1 (91.6)	98.9 (98.8)	96.3 (71.7)	98.8 (97.3)
R _{merge}	0.064 (0.18)	0.089 (0.62)	0.064 (0.47)	0.099 (0.60)
Refinement				
Rmsd from ideality				
Bond length (Å)	0.005	0.010	0.010	0.009
Bond angles (°)	1.14	1.34	1.23	1.56
R _{cryst} (R _{free})	0.208 (0.242)	0.244 (0.286)	0.204 (0.223)	0.206 (0.231)
Number of atoms				
Protein	2606	2602	2606	2606
Waters	160	82	311	81
Inhibitor	11	11	22	44
Aliphatic molecule	15	18	18	18
Average B factors (Å ²)				
Main chain	27.3	47.9	26.7	39.7
Side chain	34.9	49.5	29.5	42.2
Water	37.2	47.4	43.5	46.2
Inhibitor	48.4	72.4	53.7 (conformation A) 56.1 (conformation B)	68.1 (BCP1A) 68.5 (BCP1B) 68.2 (BCP2) 86.6 (BCP3)
Aliphatic molecule	38.3	63.2	47.8	61.0
Ramachandran plot:				
most favored	93.0 (7.0)	92.6 (7.4)	93.6 (6.4)	94.0 (6.0)
(additionally allowed)				
Wavelength (Å)	0.97930	0.91942	1.7712	1.7712
Beamline	ALS 5.0.1	APS 19ID	APS 19ID	ALS 8.2.1

from 0–2 min. Reactions were run in triplicate, and error limits on percent inhibition values are within 10%.

Crystallization of *LmGPDH*

Crystals were grown using a sitting drop vapor diffusion method by mixing 4 μl of protein solution with 4 μl of reservoir solution composed of 0.8–0.9 M sodium citrate. Crystals grew to their full size in 2 weeks. The crystals were then soaked in a cryo solution containing the corresponding inhibitor molecules for 24 hr. The cryo solutions were made of 20 mM TEA (pH 7.2), 4 mM DTT, 1 mM EDTA, 0.9 M sodium citrate, 15% (v/v) ethylene glycol, 10% DMSO, and 90 mM FCP or 60 mM BOP or 40 mM BCP. The crystals were then flash frozen and used for data collection under nitrogen stream.

Data Collection and Refinement

A data set to a resolution of 2.2 Å for the *LmGPDH*:FCP complex was collected on the SBC-CAT beam line 19-ID at the Advanced Photon Source, Argonne National Laboratory. The data for *LmGPDH*:BOP and *LmGPDH*:BCP complexes were collected to 2.3 Å and 1.9 Å resolutions, respectively, at beamline 5.0.1 of the Advanced Light Source (ALS) at the Lawrence Berkeley National Laboratory. The data were integrated, scaled, and merged with HKL2000 and SCALEPACK [38]. Intensities were transformed to amplitudes using TRUNCATE [39]. Since the crystals were isomorphous to the previous *LmGPDH* crystals upon soaking [13], the structure of the apo enzyme (1EVY.pdb) was used as the starting point for the structure refinements. After conjugate gradient minimization and restrained individual B factor refinement using the program CNS [29], sigmaA-weighted Fo-Fc maps were calculated for the three data sets and showed clear density for bound inhibitors. Second data sets for the *LmGPDH*:BOP and the *LmGPDH*:BCP complexes were collected on SBC-CAT beamline 19-ID at the Advanced Photon Source (APS) in the Argonne National Laboratory. At this time the wavelengths were chosen such that anomalous

signal from Br or Cl can be used in the determination of the orientation of bound inhibitors. After an extended X-ray absorption fine structure (EXAFS) scan for Br, *LmGPDH*:BOP data were collected at 0.91942 Å. For BCP soaked crystal, a 1.7712 Å wavelength was used for data collection (data set BCP1), because it was the longest accessible wavelength without making any time consuming changes to the instrumentation at the beamline. The data were collected for continuous 200° and 180° sweeps to achieve high overall redundancies of 15.4 and 12.9 for *LmGPDH*:BOP and *LmGPDH*:BCP, respectively, since it has been shown that high redundancy of the data is critical to utilize the small anomalous signal from light elements [40–42]. The crystals were essentially isomorphous to the apo crystal and were refined with the programs CNS and Refmac5 [43]. The structures of *LmGPDH* in complex with FCP, BOP, and BCP were refined to 2.2, 2.5, and 1.9 Å resolutions, respectively (Table 2). To clarify the identity of the anomalous peak observed in the first *LmGPDH*:BCP structure, another dataset from a different crystal was collected (data set BCP2) to 2.5 Å at ALS using a wavelength of 1.7712 Å. The third data set (BCP2) revealed a secondary binding site for BCP, where two molecules of BCP were observed between symmetry-related protein molecules. Four BCP molecules were built into the structure: BCP1A and BCP1B for the two alternative conformations in the adenosine binding site and BCP2 and BCP3 for the two molecules in the secondary binding site. Although this data helped to explain the strong anomalous peak observed in BCP1 data set, it did not give as detailed information about the binding modes of the inhibitor at the adenosine binding site, probably because of the lower resolution of the data. As in the apo structure, the initial eight residues, the last nine residues (358–366), and the loop region (294–296) of *LmGPDH* are disordered in the crystal structures and have not been included in the model. A linear saturated aliphatic molecule was built into an electron density located in a well defined hydrophobic pocket, which also appeared in the apo *LmGPDH* structure [13]. The stereochemistry of the models was verified using the software package PROCHECK [44].

Acknowledgments

We thank the members of the Biomolecular Structure Center for assistance, in particular Stewart Turley, Francis Athappilly, and Christophe Verlinde. The gene of *LmGPDH* was kindly provided by Paul Michels and Fred Opperdoes. We also thank the staffs of beamlines 5.0.1 and 8.2.1 at Advanced Light Source and the SBC-CAT at Advanced Photon Source for their kind support. Use of the Argonne National Laboratory Structural Biology Center beamlines at the Advanced Photon Source was supported by the U.S. Department of Energy, Office of Biological and Environmental Research, under Contract No. W-31-109-ENG-38. This work is supported by Grant AI44119 from the National Institutes of Health to M.H.G.

Received: July 11, 2002

Revised: September 25, 2002

Accepted: September 25, 2002

References

1. WHO. (2001). Tropical Disease Research: Progress 1999–2000, Fifteenth Programme Report.
2. Wang, C.C. (1995). Molecular mechanisms and therapeutic approaches to the treatment of African trypanosomiasis. *Annu. Rev. Pharmacol. Toxicol.* **35**, 93–127.
3. Noble, M.E., Verlinde, C.L., Groendijk, H., Kalk, K.H., Wierenga, R.K., and Hol, W.G. (1991). Crystallographic and molecular modeling studies on trypanosomal triosephosphate isomerase: a critical assessment of the predicted and observed structures of the complex with 2-phosphoglycerate. *J. Med. Chem.* **34**, 2709–2718.
4. Verlinde, C.L., Witmans, C.J., Pijning, T., Kalk, K.H., Hol, W.G., Callens, M., and Opperdoes, F.R. (1992). Structure of the complex between trypanosomal triosephosphate isomerase and N-hydroxy-4-phosphono-butanamide: binding at the active site despite an “open” flexible loop conformation. *Protein Sci.* **1**, 1578–1584.
5. Vellieux, F.M., Hajdu, J., Verlinde, C.L., Groendijk, H., Read, R.J., Greenhough, T.J., Campbell, J.W., Kalk, K.H., Littlechild, J.A., Watson, H.C., et al. (1993). Structure of glycosomal glyceraldehyde-3-phosphate dehydrogenase from *Trypanosoma brucei* determined from Laue data. *Proc. Natl. Acad. Sci. USA* **90**, 2355–2359.
6. Verlinde, C.L., and Hol, W.G. (1994). Structure-based drug design: progress, results and challenges. *Structure* **2**, 577–587.
7. Kim, H., Feil, I.K., Verlinde, C.L., Petra, P.H., and Hol, W.G. (1995). Crystal structure of glycosomal glyceraldehyde-3-phosphate dehydrogenase from *Leishmania mexicana*: implications for structure-based drug design and a new position for the inorganic phosphate binding site. *Biochemistry* **34**, 14975–14986.
8. Bernstein, B.E., Michels, P.A., and Hol, W.G. (1997). Synergistic effects of substrate-induced conformational changes in phosphoglycerate kinase activation. *Nature* **385**, 275–278.
9. Aronov, A.M., Suresh, S., Buckner, F.S., Van Voorhis, W.C., Verlinde, C.L., Opperdoes, F.R., Hol, W.G., and Gelb, M.H. (1999). Structure-based design of submicromolar, biologically active inhibitors of trypanosomatid glyceraldehyde-3-phosphate dehydrogenase. *Proc. Natl. Acad. Sci. USA* **96**, 4273–4278.
10. Bressi, J.C., Verlinde, C.L., Aronov, A.M., Shaw, M.L., Shin, S.S., Nguyen, L.N., Suresh, S., Buckner, F.S., Van Voorhis, W.C., Kuntz, I.D., et al. (2001). Adenosine analogues as selective inhibitors of glyceraldehyde-3-phosphate dehydrogenase of Trypanosomatidae via structure-based drug design. *J. Med. Chem.* **44**, 2080–2093.
11. Bressi, J.C., Choe, J., Hough, M.T., Buckner, F.S., Van Voorhis, W.C., Verlinde, C.L., Hol, W.G., and Gelb, M.H. (2000). Adenosine analogues as inhibitors of *Trypanosoma brucei* phosphoglycerate kinase: elucidation of a novel binding mode for a 2-amino-N(6)-substituted adenosine. *J. Med. Chem.* **43**, 4135–4150.
12. Chudzik, D.M., Michels, P.A., de Walque, S., and Hol, W.G. (2000). Structures of type 2 peroxisomal targeting signals in two trypanosomatid aldolases. *J. Mol. Biol.* **300**, 697–707.
13. Suresh, S., Turley, S., Opperdoes, F.R., Michels, P.A., and Hol, W.G. (2000). A potential target enzyme for trypanocidal drugs revealed by the crystal structure of NAD-dependent glyceraldehyde-3-phosphate dehydrogenase from *Leishmania mexicana*. *Struct. Fold. Des.* **8**, 541–552.
14. Suresh, S., Bressi, J.C., Kennedy, K.J., Verlinde, C.L., Gelb, M.H., and Hol, W.G. (2001). Conformational changes in *Leishmania mexicana* glyceraldehyde-3-phosphate dehydrogenase induced by designed inhibitors. *J. Mol. Biol.* **309**, 423–435.
15. Opperdoes, F.R. (1987). Compartmentation of carbohydrate metabolism in trypanosomes. *Annu. Rev. Microbiol.* **41**, 127–151.
16. Michels, P.A., Hannaert, V., and Bringaud, F. (2000). Metabolic aspects of glycosomes in trypanosomatidae—new data and views. *Parasitol. Today* **16**, 482–489.
17. Bakker, B.M., Michels, P.A.M., Opperdoes, F.R., and Westerhoff, H.V. (1997). Glycolysis in bloodstream form *Trypanosoma brucei* can be understood in terms of the kinetics of the glycolytic enzymes. *J. Biol. Chem.* **272**, 3207–3215.
18. Bakker, B.M., Michels, P.A., Opperdoes, F.R., and Westerhoff, H.V. (1999). What controls glycolysis in bloodstream form *Trypanosoma brucei*? *J. Biol. Chem.* **274**, 14551–14559.
19. Bakker, B.M., Walsh, M.C., ter Kuile, B.H., Mensonides, F.I., Michels, P.A., Opperdoes, F.R., and Westerhoff, H.V. (1999). Contribution of glucose transport to the control of the glycolytic flux in *Trypanosoma brucei*. *Proc. Natl. Acad. Sci. USA* **96**, 10098–10103.
20. Bakker, B.M., Westerhoff, H.V., Opperdoes, F.R., and Michels, P.A. (2000). Metabolic control analysis of glycolysis in trypanosomes as an approach to improve selectivity and effectiveness of drugs. *Mol. Biochem. Parasitol.* **106**, 1–10.
21. Aronov, A.M., Verlinde, C.L., Hol, W.G., and Gelb, M.H. (1998). Selective tight binding inhibitors of trypanosomal glyceraldehyde-3-phosphate dehydrogenase via structure-based drug design. *J. Med. Chem.* **41**, 4790–4799.
22. Denise, H., Giroud, C., Barrett, M.P., and Baltz, T. (1999). Affinity chromatography using trypanocidal arsenical drugs identifies a specific interaction between glyceraldehyde-3-phosphate dehydrogenase from *Trypanosoma brucei* and Cymelarsan. *Eur. J. Biochem.* **259**, 339–346.
23. Lo, T.W., Westwood, M.E., McLellan, A.C., Selwood, T., and Thormalley, P.J. (1994). Binding and modification of proteins by methylglyoxal under physiological conditions. A kinetic and mechanistic study with N alpha-acetylarginine, N alpha-acetylcysteine, and N alpha-acetyllysine, and bovine serum albumin. *J. Biol. Chem.* **269**, 32299–32305.
24. Coombs, G.H., Craft, J.A., and Hart, D.T. (1982). A comparative study of *Leishmania mexicana* amastigotes and promastigotes. Enzyme activities and subcellular locations. *Mol. Biochem. Parasitol.* **5**, 199–211.
25. Marche, S., Michels, P.A., and Opperdoes, F.R. (2000). Comparative study of *Leishmania mexicana* and *Trypanosoma brucei* NAD-dependent glyceraldehyde-3-phosphate dehydrogenase. *Mol. Biochem. Parasitol.* **106**, 83–91.
26. Tereshko, V., Wilds, C.J., Minasov, G., Prakash, T.P., Maier, M.A., Howard, A., Wawrzak, Z., Manoharan, M., and Egli, M. (2001). Detection of alkali metal ions in DNA crystals using state-of-the-art X-ray diffraction experiments. *Nucleic Acids Res.* **29**, 1208–1215.
27. Dauter, Z., and Adamski, D.A. (2001). Anomalous signal of phosphorus used for phasing DNA oligomer: importance of data redundancy. *Acta Crystallogr. D Biol. Crystallogr.* **57**, 990–995.
28. de Graaff, R.A., Hilge, M., van der Plas, J.L., and Abrahams, J.P. (2001). Matrix methods for solving protein substructures of chlorine and sulfur from anomalous data. *Acta Crystallogr. D Biol. Crystallogr.* **57**, 1857–1862.
29. Brunger, A.T., Adams, P.D., Clore, G.M., DeLano, W.L., Gros, P., Grosse-Kunstleve, R.W., Jiang, J.S., Kuszewski, J., Nilges, M., Pannu, N.S., et al. (1998). Crystallography & NMR system: a new software suite for macromolecular structure determination. *Acta Crystallogr. D Biol. Crystallogr.* **54**, 905–921.
30. Hendrickson, W.A., and Teeter, M.M. (1981). Structure of the hydrophobic protein crambin determined directly from the anomalous scattering of sulfur. *Nature* **290**, 107–113.

31. Cromer, D.T. (1983). Calculations of anomalous scattering factors at arbitrary wavelengths. *J. Appl. Crystallogr.* **16**, 437–438.
32. Brennan, S., and Cowan, P.L. (1992). A suite of programs for calculating x-ray absorption, reflection and diffraction performance for a variety of materials at arbitrary wavelengths. *Rev. Sci. Instrum.* **63**, 850.
33. CCP4 (Collaborative Computational Project Number 4) (1994). The CCP4 suite: programs for protein crystallography. *Acta Crystallogr. D* **50**, 760–763.
34. Beaman, A.G., Gerster, J.F., and Robins, R.K. (1961). Potential purine antagonists. XXVIII. The preparation of various bromo-purines. *J. Org. Chem.* **27**, 986–990.
35. Wright, G.E., Dudycz, L.W., Kazimierczuk, Z., Brown, N.C., and Khan, N.N. (1987). Synthesis, cell growth inhibition, and antitumor screening of 2-(p-n-butylanilino)purines and their nucleoside analogues. *J. Med. Chem.* **30**, 109–116.
36. Gray, N.S., Kwon, S., and Schultz, P.G. (1997). Combinatorial synthesis of 2,9-substituted purines. *Tetrahedron Lett.* **38**, 1161–1164.
37. Kohl, L., Drmota, T., Thi, C.D., Callens, M., Van Beeumen, J., Opperdoes, F.R., and Michels, P.A. (1996). Cloning and characterization of the NAD-linked glycerol-3-phosphate dehydrogenases of *Trypanosoma brucei brucei* and *Leishmania mexicana mexicana* and expression of the trypanosome enzyme in *Escherichia coli*. *Mol. Biochem. Parasitol.* **76**, 159–173.
38. Otwinowski, Z.M., and Minor, W. (1997). Processing of X-ray diffraction data collected in oscillation mode. *Methods Enzymol.* **276**, 307–326.
39. French, G.S., and Wilson, K.S. (1978). On the treatment of negative intensity observations. *Acta Crystallogr. A* **34**, 517–525.
40. Dauter, Z., Dauter, M., de La Fortelle, E., Bricogne, G., and Sheldrick, G.M. (1999). Can anomalous signal of sulfur become a tool for solving protein crystal structures? *J. Mol. Biol.* **289**, 83–92.
41. Weiss, M.S., Sicker, T., and Hilgenfeld, R. (2001). Soft X-rays, high redundancy, and proper scaling: a new procedure for automated protein structure determination via SAS. *Structure* **9**, 771–777.
42. Liu, Z.J., Vysotski, E.S., Chen, C.J., Rose, J.P., Lee, J., and Wang, B.C. (2000). Structure of the Ca²⁺-regulated photoprotein obelin at 1.7 Å resolution determined directly from its sulfur substructure. *Protein Sci.* **9**, 2085–2093.
43. Murshudov, G.N., Vagin, A.A., and Dodson, E.J. (1997). Refinement of macromolecular structures by the maximum-likelihood method. *Acta Crystallogr. D* **53**, 240–255.
44. Laskowski, R.A., MacArthur, M.W., Moss, D.S., and Thornton, J.M. (1993). PROCHECK: a program to check the stereochemical quality of protein structures. *J. Appl. Crystallogr.* **26**, 283–291.
45. Kraulis, P. (1991). MOLSCRIPT: a program to produce both detailed and schematic plots of protein structures. *J. Appl. Crystallogr.* **24**, 946–950.
46. Merritt, E.A., and Bacon, D.J. (1997). Raster3D: photorealistic molecular graphics. *Methods Enzymol.* **277**, 505–524.